THE MAGNETIC FIELD OF A SINGLE AXON

A Comparison of Theory and Experiment

BRADLEY J. ROTH AND JOHN P. WIKSWO, JR.
Department of Physics and Astronomy, Vanderbilt University, Nashville, Tennessee 37235

ABSTRACT The magnetic field and the transmembrane action potential of a single nerve axon were measured simultaneously. The volume conductor model was used to calculate the magnetic field from the measured action potential, allowing comparison of the model predictions with the experimental data. After analyzing the experiment for all systematic errors, we conclude that the shape of the magnetic field can be accurately predicted from the transmembrane potential and, more importantly, the shape of the transmembrane potential can be calculated from the magnetic field. The data are used to determine r_i, the internal resistance per unit length of the axon, to be 19.3 ± 1.9 kΩ mm^{-1}, implying a value for the internal conductivity of 1.44 ± 0.33 $\Omega^{-1}\ m^{-1}$. Magnetic measurements are compared with standard bioelectric techniques for studying nerve axons.

INTRODUCTION

An active nerve axon can be modeled with sufficient accuracy to allow a detailed calculation of the associated magnetic field. Therefore the single axon provides a simple, yet fundamentally important system from which we can test our understanding of the relation between biomagnetic and bioelectric fields. The magnetic field produced by a propagating action potential has been calculated from the transmembrane action potential using the volume conductor model (1). The purpose of this paper is to verify that calculation experimentally. To make an accurate comparison between theory and experiment, we must be careful to correct for all systematic errors present in the data.

To test the volume conductor model it is necessary to measure the transmembrane potential and the magnetic field simultaneously. An experiment performed by Wikswo et al. (2) provided preliminary data from a lobster axon, however the electric and magnetic signals were recorded at different positions along the axon and no quantitative comparisons were made between theory and experiment. In the experiment reported here, these limitations were overcome and improved instrumentation was used (3–5).

GLOSSARY

σ_e the external conductivity of the bath
σ_i the internal conductivity of the axoplasm
u the conduction velocity
a the axon radius
ρ the field point radius.

REVIEW OF THE VOLUME CONDUCTOR MODEL

With some simplifying assumptions the magnetic field produced by an axon can be calculated from the transmembrane potential using the volume conductor model. This calculation is outlined in Appendix A and more fully as described in reference 1. It requires solving Laplace's equation for the electrical potential, then using Ohm's law to find the current density and Ampere's law to find the magnetic field. We assume that the axon is a uniform, infinitely long cylindrical membrane immersed in an unbounded conducting bath, the action potential propagates with a uniform velocity down the axon, the conducting media are linear, isotropic, homogeneous, and quasistatic, and the transmembrane potential is cylindrically symmetric. The calculation requires that the transmembrane potential be given, along with the five parameters given in the Glossary. Since these quantities are either measured or obtained from the literature, the model has no free parameters.

When the spatial length of the depolarization phase of the action potential, Δz, is much greater than the axon radius, and when the resistance of the bath is small compared with the internal resistance of the axon, the results of the volume conductor model are easy to summarize. The magnetic field is nearly independent of σ_e, and is proportional to $\sigma_i \pi a^2$, or inversely proportional to the internal resistance of the axon per unit length, $r_i = 1/\sigma_i \pi a^2$.

Address reprint requests to John P. Wikswo, Jr., Department of Physics and Astronomy, Vanderbilt University, Box 1807 Station B, Nashville, TN 37235.

The dependence of the magnetic field on the field point radius and the conduction velocity can be understood using Ampere's law, which states that the magnetic field at a distance ρ from the axon is proportional to the net current passing through a circle of radius ρ around the axon. The net current is the sum of the current inside the axon and the fraction of the extracellular current passing through the circle, referred to as the return current.

The spatial distribution of the current in the bath is determined by the length of the depolarization phase of the action potential. If the field point radius ρ is small, so that $\rho << \Delta z$, then the contribution of the return current is negligible, and the magnetic field is proportional to the current inside the axon, which is in turn proportional to the first derivative of the transmembrane potential. If the measuring point is far from the nerve, $\rho >> \Delta z$, the return current will almost completely cancel the internal current, so that the magnetic field will be smaller in amplitude and broadened, containing much less high frequency information. In this case a multipole expansion of the current density is useful in approximating the magnetic field. When $\rho \approx \Delta z$ no simple approximation is adequate and the full power of the volume conductor model is required to accurately calculate the magnetic field. Thus Δz is a key parameter as it sets the length scale of the problem. It is determined by the rise time and conduction velocity of the action potential. In this experiment $\Delta z \approx 3$ mm. The significance of all other distances is determined primarily by their size relative to Δz.

The calculation, as outlined in Appendix A, can be inverted to compute the transmembrane potential from the magnetic field. This computation is difficult, however, because the equation giving the transmembrane potential from the magnetic field strongly emphasizes the high frequency components of the signal. Thus the inverse calculation requires additional low-pass filtering if any high frequency noise is present in the magnetic data.

DESCRIPTION OF THE EXPERIMENT

An experiment was performed to test the validity of the calculation of the magnetic field using the volume conductor model. The data were obtained from a medial giant axon of a crayfish. The crayfish was dissected in oxygenated, circulating Van Harreveld's solution, Tris buffered to a pH of 7.4, at 5°C. The appendages and exoskeleton were removed, and the muscle and chitin dorsal to the nerve bundle were cleared away. The ends of the bundle were ligated, the chord was freed from peripheral nerve fibers, and the entire nerve bundle was transferred to the experimental apparatus.

A schematic diagram of the experiment is shown in Fig. 1. The nerve was threaded through a toroidal pick-up coil to the fifth thoracic ganglion, where the data were taken. The esophogeal connectives were placed in separate insulated Plexiglas troughs, each containing a stimulating electrode so that either medial giant axon could be stimulated individually. The distance from the toroid to the point of stimulation was ~20 mm. The nerve chord, as well as the toroid and stimulating electrodes, were submerged in a bath of circulating Van Harreveld's solution at room temperature.

The magnetic signal was sensed inductively using the toroidal pick-up coil, which consisted of a ferrite core toroid wound with 65 evenly spaced

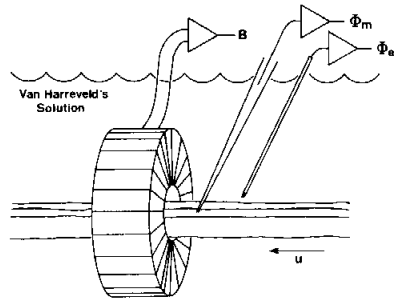

FIGURE 1 Schematic diagram of the experiment.

turns of 40 gauge (0.074 mm diameter) copper wire. The toroid was threaded by both the axon and a single-turn calibration wire carrying a 1 μA, 0.5-ms square calibration pulse before each stimulation. The ferrite core had a square cross section, with an inner radius of 1.05 mm, an outer radius of 1.95 mm, and a width of 1.25 mm. It was insulated from the bath by a coating of epoxy, so that the encapsulated coil had an inner radius of 0.75 mm, an outer radius of 2.25 mm, and a width of 1.90 mm. Fig. 2 summarizes the toroid geometry. The current induced in the 65-turn toroid winding was sensed by a room temperature, low-noise amplifier (5), and a frequency compensator was used to correct for the frequency response of the toroid and amplifier system (3). The signal was then filtered (50 kHz low pass), digitized with an 8 μs sampling period, averaged, and displayed by a signal averager (model 1170; Nicolet Instrument Corp., Madison, WI). Fig. 3 *a* shows a recording of the digitized magnetic signal without averaging or digital filtering.

The transmembrane potential was recorded using a glass microelectrode filled with 1 M potassium chloride, having an impedance of ~20 MΩ. The microelectrode was inserted through the nerve bundle sheath into the left medial giant axon 1 mm from the center of the toroid. Upon insertion of the microelectrode at the beginning of the experiment and upon the removal of the microelectrode at the end of the experiment a resting potential of about −75 mV was observed. The microelectrode signal was calibrated using a 10 mV, 0.3 ms square voltage pulse applied to the bath through the ground wire. The frequency response of the microelectrode was compromised to some extent by the requirement that the axon was 6 mm below the surface of the bath, thereby producing a distributed microelectrode tip capacitance. We compensated for this by injecting a square pulse of current (0.5 ms, ~1 nA) into the microelec-

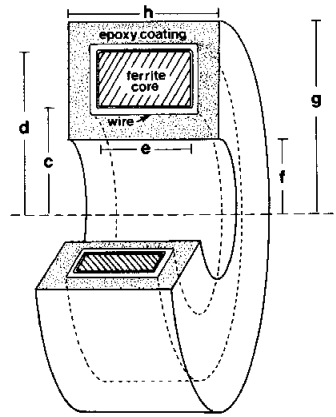

FIGURE 2 Geometry of the toroid; c = 1.05 mm, d = 1.95 mm, e = 1.25 mm, f = 0.75 mm, g = 2.25 mm, and h = 1.90 mm.

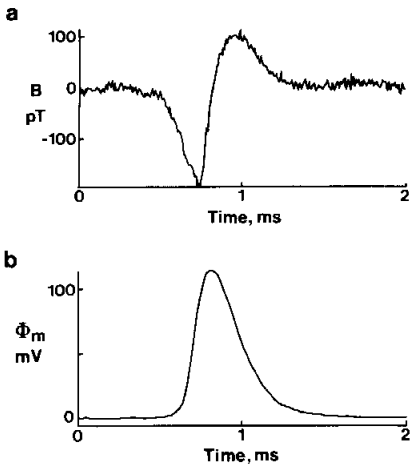

FIGURE 3 (*a*) The measured magnetic field, (*b*) the measured transmembrane potential. In both cases no signal averaging was used.

trode and adjusting the negative capacitance circuit in the microelectrode electrometer (model M701; World Precision Instruments, Inc., New Haven, CT) until the best possible square voltage pulse was observed. In this way we were able to extend the bandwidth of the microelectrode until the leading edge of the pulse had a rise time of 50 μs. The accuracy with which both the microelectrode and the toroid output were corrected for their frequency response provides one limitation to the accuracy of our data. We estimate that we were able to perform the frequency compensation so that the shape and amplitude of the measured signals were accurate to within 2%. The microelectrode signal was then filtered (50 kHz low pass), averaged and recorded by the Nicolet signal averager (Nicolet Instrument Corp.). Fig. 3 *b* shows the transmembrane potential with no averaging.

The potential difference between a tungsten electrode 200 μm from the axon center and a silver-silver chloride ground electrode ~30 mm from the axon was also recorded. The tungsten electrode tip had a diameter of 100 μm and was 100 μm long, the rest of the electrode being insulated from the bath. The electrode was held in place 2.5 mm from the toroid by a micropositioner. The radial distance from the center of the axon to the center of the exposed tungsten tip was measured by carefully placing the electrode just in contact with the nerve bundle, and then backing the electrode away until the desired field point was reached. The same 10-mV pulse used to calibrate the microelectrode signal was also used for calibration of the external potential. The signal was amplified by a low noise pre-amplifier (model 113; EG & G Princeton Applied Research Corp., Princeton, NJ), and then filtered (50 kHz low pass) and averaged by the Nicolet signal averager (Nicolet Instrument Corp.)

The nerve was stimulated at a rate of about twice per second. The exact frequency of stimulation (1.967 Hz) was timed so that 60-Hz noise and all its odd harmonics would be absent in the averaged data (3). The strength of the stimulus was just above threshold. Stimulus artifact could easily be canceled from the magnetic signal (3).

COMPARISON OF THEORY AND DATA

Using the measured transmembrane potential and the parameters $a = 0.107$ mm, $\sigma_i = 1.70\,\Omega^{-1}\,m^{-1}$, $\sigma_e = 2.06\,\Omega^{-1}\,m^{-1}$, $u = 16.5$ m/s and $\rho = 1.48$ mm, we obtain a theoretical magnetic field that is compared with the measured magnetic field (512 averages) in Fig. 4. The signals have been plotted with different vertical scales, so that the shape of the trace can be compared more easily. One discrepancy between theory and experiment is that the fields have different amplitudes. The calculated signal has a peak-to-peak amplitude 17% larger than the experimental data. There are also differences between the shapes of the signals. The measured magnetic signal is narrower than the theoretical prediction, the full width at half maximum (FWHM) of the depolarization phase differing by 12%. The ratio of the amplitude of the depolarization phase to repolarization phase, or the asymmetry of the signal, disagree by 3%, the measured data being more asymmetric. The differences between the shape of the calculated and measured magnetic fields were consistent for several different axons, while the variation in the amplitude was not as consistent. These discrepancies will be examined in detail later in this paper.

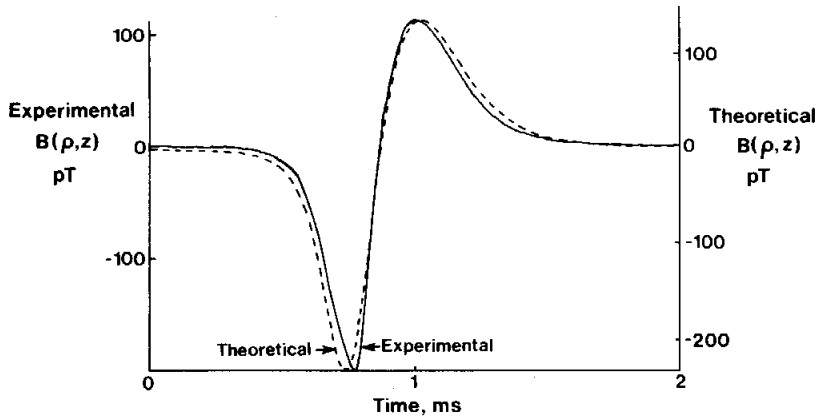

FIGURE 4 A comparison of the measured magnetic field (solid) and that calculated from the transmembrane potential (dashed). The measured signal represents 512 averages. Note the different vertical scales. $a = 0.107$ mm, $\sigma_i = 1.70\,\Omega^{-1}\,m^{-1}$, $\sigma_e = 2.06\,\Omega^{-1}\,m^{-1}$, $\rho = 1.48$ mm, $u = 16.5$ m/s.

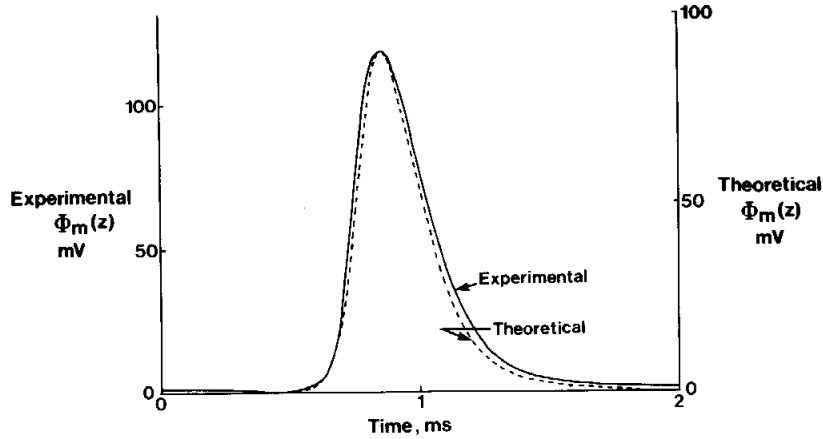

FIGURE 5 A comparison of the measured transmembrane potential (solid) and the transmembrane potential calculated from the magnetic field (dashed). The measured signal represents 512 averages. Note the different vertical scales. $a = 0.107$ mm, $\sigma_i = 1.70\,\Omega^{-1}\,m^{-1}$, $\sigma_e = 2.06\,\Omega^{-1}\,m^{-1}$, $\rho = 1.48$ mm, $u = 16.5$ m/s.

In Fig. 5 we also show the result of the inverse calculation, comparing the measured transmembrane potential (512 averages) to that calculated from the magnetic field. We perform the necessary low-pass filtering by multiplying the Fourier transform of the calculated signal by a Tukey window ($k_1 = 0.0\ mm^{-1}$, $k_2 = 4.0\ mm^{-1}$) (1). These values of k_1 and k_2 imply that there are no contributions to the calculated transmembrane potential above 10 kHz. For subsequent comparisons between theory and experiment we shall concentrate on the magnetic field, not the transmembrane potential, to eliminate any effects due to low-pass filtering.

SYSTEMATIC ERRORS IN THE EXPERIMENT

There are several systematic errors in the experiment. We shall examine each source of error individually, determining the change it will produce in the magnetic field. Two criteria will be used to characterize the magnetic signal: the peak-to-peak amplitude and the FWHM of the depolarization phase.

We can organize the possible systematic errors into four classes. First, the values of the parameters required by the volume conductor model may be inaccurate. We must determine how accurately each parameter is known, and how their uncertainties propagate through the calculation of the magnetic field. Second, the toroid does not measure the magnetic field at a single point. We will examine the averaging of the magnetic field over the cross section of the ferrite core, and the averaging of the magnetic field over all angles. A third class of errors is due to inhomogeneities in the conductivity of the external medium. Three such inhomogeneities are considered: the bounded bath, the nerve bundle, and the toroid. Finally, there are several remaining systematic errors, such as the deviation of the axon geometry from the model assumptions, which are harder to assess.

Parameters of the Volume Conductor Model

The determination of the five parameters required by the volume conductor model represents the major source of error in the experiment. Of the five parameters, the model is least sensitive to the external conductivity. We measured the conductivity of the Van Harreveld's solution to be 2.06 $\pm$ 0.10 $\Omega^{-1}\,m^{-1}$ by using a conductance meter (model 35; Yellow Springs Instrument Co., Yellow Springs, OH). The 5% uncertainty in σ_e leads to only a 0.1% uncertainty in the magnetic field.

We measured the conduction velocity to be $u = 16.5 \pm 1.6$ m/s, achieving 10% accuracy by using two toroids separated by a known distance (6 mm). (We demonstrated experimentally that the presence of one toroid had no effect on the magnetic signal measured by the other for toroid separations >3 mm). Implicit in our measurement is the assumption that the conduction velocity is constant along the length of the axon between the toroids. The 10% uncertainty in the conduction velocity could account for 4% of the discrepancy in the peak-to-peak amplitude of the theoretical and experimental signals. Also, of the five parameters, the shape of the magnetic signal is most sensitive to u; its uncertainty could lead to a 3% change in the FWHM of the calculated magnetic field.

The value of the field point radius ρ was selected to be a representative point inside the toroid, $\rho = 1.48 \pm 0.07$ mm. More will be said on how this value of ρ was determined when systematic errors due to the toroid are discussed. The 5% uncertainty in ρ leads to an 8% uncertainty in the peak-to-peak amplitude of the magnetic field and a 2% change in the FWHM.

The axon radius, $a = 0.107 \pm 0.011$ mm, was measured to 10% accuracy by observing it under a microscope at a magnification of 120. The radius varied by ~10% over distances <1 mm, so an average radius was measured near the microelectrode penetration. In this measurement we assume that the axon has a circular cross section. The magnetic field is proportional to the axon radius squared, so a 10% uncertainty in the axon radius will produce a 20% uncertainty in the peak-to-peak amplitude of the magnetic signal. The change in the FWHM of the magnetic signal will be <1%, the shape of the magnetic field being a very weak function of a.

The internal conductivity is the only parameter that was not directly measured. We obtained our value from Hodgkin and Rushton's work on a lobster axon (6), in which they found $\sigma_i = 1.7 \pm 0.5\ \Omega^{-1}\ m^{-1}$. The 30% uncertainty arose from random error in their experiment, and is an expression of the difficulty encountered when determining σ_i from subthreshold electrotonic measurements. In using this value for our calculation we assume that the axoplasm of lobsters and crayfish have similar conductivities. Watanabe and Grundfest (7) independently estimate the internal conductivity of a crayfish lateral giant axon as $\sim 1.1\ \Omega^{-1}\ m^{-1}$, but they express skepticism about their accuracy. We adopt 1.7 as our value of σ_i, realizing that this number could be very inaccurate. We expect the true value actually falls within 50% of our estimate, or $\sigma_i = 1.70 \pm 0.85\ \Omega^{-1}\ m^{-1}$. The magnetic field is proportional to σ_i, therefore there is a corresponding 50% uncertainty in the peak-to-peak amplitude of the magnetic signal. In determining the shape of the magnetic signal, the internal conductivity enters the equations of the volume conductor model in much the same way as does the external conductivity. Therefore, there is only a weak dependence of the shape of the signal on σ_i, a 50% uncertainty in the internal conductivity producing <1% uncertainty in the FWHM of the magnetic signal.

We can combine σ_i and a into one parameter, the axon's internal resistance per unit length, $r_i = 16.4 \pm 8.8$ kΩ mm^{-1}. We know r_i and therefore the amplitude of the calculated magnetic field to no better than 50%. Thus, the 17% discrepancy between the peak-to-peak amplitude of our theoretical and measured magnetic fields can be totally explained by uncertainty in the axon resistance. The shape of the magnetic signal is insensitive to r_i, so that even a 50% uncertainty in r_i produces a uncertainty in the shape (FWHM) of the signal of <1%. If we had calculated the magnetic field from the axial current, not the transmembrane potential, the strong dependence of the amplitude of the magnetic field on r_i would not have appeared, eliminating the dominant source of error in our experiment. Magnetic measurements are therefore particularly well suited for measuring currents in biological systems. If both the magnetic field and the transmembrane potential are measured, then we can use our model to predict r_i, introducing one free parameter with which we can fit the theoretical predictions to data. For this particular crayfish, the peak-to-peak amplitude of the theoretical and experimental magnetic fields are equal for $r_i = 19.3 \pm 1.9$ kΩ mm^{-1}, the 10% uncertainty being primarily due to the uncertainty in ρ and u. It is often convenient to consider the free parameter to be the internal conductivity, since this is the only parameter not directly measured. Using $a = 0.107 \pm 0.011$ mm for the axon radius, we calculate σ_i to be $1.44 \pm 0.33\ \Omega^{-1}\ m^{-1}$. The 23% uncertainty, primarily due to the uncertainty in a, is somewhat smaller than would be obtained from electrotonic measurements. A more precise measurement of a would reduce the uncertainty in σ_i significantly.

We see that uncertainties in the volume conductor model parameters can account for many of the differences between theory and experiment. To explain the remaining discrepancies, we must look for systematic errors in the experiment design.

Toroid Effects

The toroid that senses the magnetic field introduces two systematic errors into the experiment because it does not measure the magnetic field at a single point. Instead, it averages the magnetic field over all angles θ and over the toroid cross section. The mutual inductance between the toroid and the axon is negligible, and effects due to the presence of the high permeability ferrite core should be small.

Averaging Over All Angles θ. The magnetic field we measure with our toroid, $\bar{B}(\rho, z)$, is the tangential component B^θ of the magnetic field averaged over all angles

$$\bar{B}(\rho, z) = \frac{\int_0^{2\pi} B^\theta(\rho, \theta, z)\mathrm{d}\theta}{\int_0^{2\pi} \mathrm{d}\theta}. \tag{1}$$

We can gain some insight into how this averaging affects our data by using Ampere's law, which relates the measured magnetic field to I_{enclosed}, the net current passing through the toroid. If there is cylindrical symmetry, then Ampere's law reduces to (Appendix A)

$$B(\rho, z) = \frac{\mu_0}{2\pi\rho} I_{\text{enclosed}}, \tag{2}$$

so the magnetic field is simply proportional to I_{enclosed}. If there is not cylindrical symmetry, Ampere's law still simplifies to a similar result, but in this case involving the average magnetic field $\bar{B}$

$$\bar{B}(\rho, z) = \frac{\mu_0}{2\pi\rho} I_{\text{enclosed}}. \tag{3}$$

Therefore, we obtain the same result in a noncylindrically symmetric case as we do in a cylindrically symmetric one if we replace B by $\bar{B}$. It follows that the magnetic field we

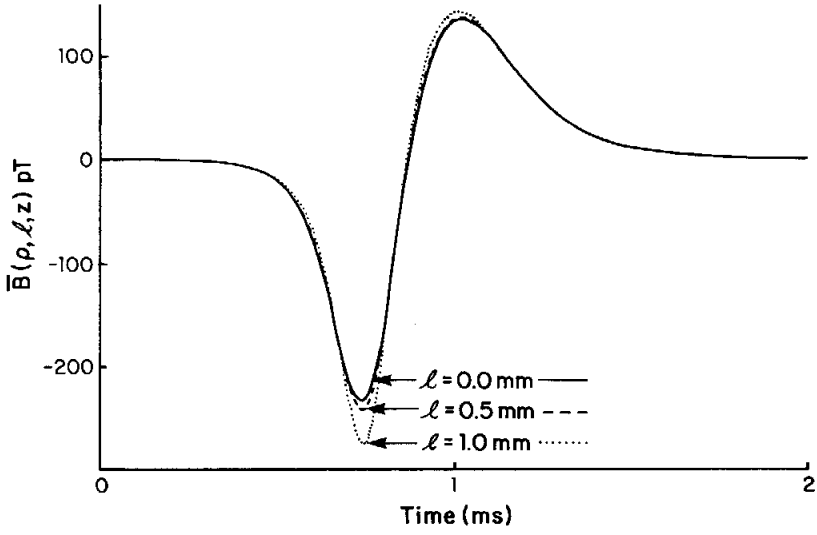

FIGURE 6 The magnetic field corrected for the axon being off-axis in the toroid. The distance off-axis, ℓ, is equal to 0.0, 0.5, and 1.0 mm for the three traces. $a = 0.107$ mm, $\sigma_i = 1.70\ \Omega^{-1}\ m^{-1}$, $\sigma_e = 2.06\ \Omega^{-1}\ m^{-1}$, $\rho = 1.48$ mm, $u = 16.5$ m/s.

measure depends only on the net current threading the toroid and not on how that current is distributed. Thus, the calibration wire does not need to lie in the center of the toroid, but can be placed along the inner radius of the ferrite core; the total current threading the toroid is independent of its position. (We experimentally verified that the measured magnetic field is independent of the position of the calibration wire in the toroid.) However, we cannot assume that the nerve may also lie anywhere in the toroid because a change in the position of the axon may shift the external current density in such a way as to alter the return current. Therefore if the axon did not lie exactly on-axis in the toroid, then a systematic error may exist in our data.

We show in Appendix B that the volume conductor model can be extended to calculate the magnetic field due to the axon being off-axis in the toroid. The results of this calculation are shown in Fig. 6, where the average magnetic field is plotted for several values of the parameter ℓ, the distance between the center of the axon and the center of the toroid. For $\ell = 1$ mm, which places the nerve near the inner surface of the toroid core,[1] the peak-to-peak amplitude of the magnetic signal increases by 17%. In our experiment, the axon was supported by the nerve bundle so that ℓ was small. We estimate $\ell < 0.3$ mm, implying that the maximum error in the peak-to-peak amplitude due to the axon being off-axis in the toroid is 2%, while the error in the FWHM is <1%.

[1]For this theoretical calculation we ignore the epoxy coating around the ferrite core so that the axon can be placed 1 mm from the toroid center.

Averaging Over the Toroid Cross Section. The averaging of the magnetic field over the ferrite core cross section represents a second systematic error introduced by the toroid. Whenever the width or radius of the toroid becomes comparable to or larger than the depolarization length of the action potential, this averaging will change the magnetic signal significantly. The volume conductor model can again be extended to calculate the average field. In Appendix C we show that the effect of averaging the magnetic field over the toroid cross section can be approximated to within 1% by assigning an effective field point radius, ρ_{eff}. For the ferrite core used in this study, the inner radius, c, was 1.05 mm, the outer radius, d, was 1.95 mm and the width, e, was 1.25 mm (Fig. 2), giving $\rho_{eff} = 1.48$ mm. It was this value of ρ that we used in Fig. 4 to calculate the magnetic field from the transmembrane potential. Since we can measure the toroid dimensions c, d, and e carefully (to within 5%) before the experiment, we feel confident in the accuracy of ρ_{eff} to the same precision, or $\rho_{eff} = 1.48 \pm 0.07$ mm.

Inductive Effects. Through the assumption of quasistationarity, the volume conductor model neglects inductive effects. Plonsey and Heppner (8) have discussed the conditions under which this approximation is valid. However, their arguments do not consider the presence of the high permeability toroid encircling the axon, in which the magnetic field is magnified by a factor of 10^4 ($\mu \approx 10^4\ \mu_0$). We shall show that inductive effects are still completely negligible even when the toroid is present.

To verify our claim we shall calculate the order of magnitude of the inductively induced electric field.

Because of the identical form of the two Maxwell's equations (ignoring displacement currents)

$$\nabla \times \mathbf{E} = -\frac{\partial \mathbf{B}}{\partial t} \qquad \nabla \times \mathbf{B} = \mu_0 \mathbf{J} \tag{4}$$

we can consider the toroid as a ring of changing magnetic flux that will produce an electric field in exact analogy to the production of a magnetic field by a current loop. The magnetic field at the center of a circular current loop is derived in many elementary texts on electricity and magnetism (9), and is

$$B = \frac{\mu_0 I}{2\rho}. \tag{5}$$

By analogy, the electric field induced by the toroid is

$$E = -\frac{\frac{\partial \Phi_B}{\partial t}}{2\rho}, \tag{6}$$

where Φ_B is the magnetic flux through the toroid cross section, and ρ is the toroid radius. The magnetic field changes by 200 pT in 0.1 ms. The toroid cross section is ~1 mm^2 and the radius is ~1 mm, so the electric field is

$$E \approx \frac{(10^4)(200\text{ pT})(1\text{ mm}^2)}{(2)(0.1\text{ ms})(1\text{ mm})} = 10^{-5}\frac{\text{V}}{\text{m}}. \tag{7}$$

But the electric field already existing due to the presence of electric charge is

$$E = -\nabla\Phi \approx \frac{100\text{ mV}}{1\text{ mm}} = 10^2\frac{\text{V}}{\text{m}}. \tag{8}$$

We conclude that inductive effects are negligible to one part in 10^7. Expressing our result in terms of circuit elements instead of fields, we can say that the mutual inductance between the toroid and the axon does not significantly change the impedance of the nerve.

High Permeability Ferrite Core. As long as the behavior of the high permeability material in the toroid is linear and the magnetic field lines are always parallel to the toroid surface, there will be no distortion of the magnetic field such as crowding of the field lines into the ferrite core. Since we deal with such small fields it is valid to assume that the ferrite behaves linearly. If the toroid is skewed with respect to the z-axis so that the plane of the toroid is not perpendicular to the axis of the axon, then additional boundary conditions for the normal and tangential components of the magnetic field at the ferrite surface must be met and the field may be distorted. In our experiment the plane of the toroid was positioned as nearly perpendicular to the axis of the axon as possible. We assume that a small misalignment of the toroid will not significantly alter the measured signal.

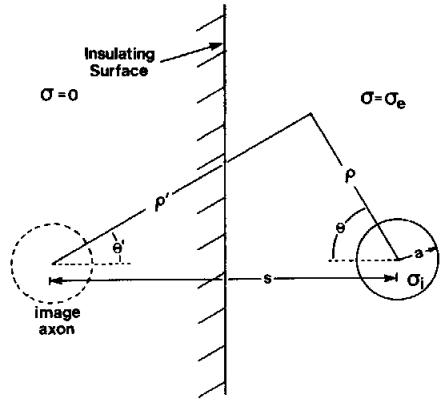

FIGURE 7 The geometry for an axon adjacent to an insulating plane surface. The dotted circle represents the image axon.

Inhomogeneities in the External Medium

Another source of systematic error in the experiment is inhomogeneities in the electrical conductivity of the external medium. These inhomogeneities provide additional boundary conditions in the original electrostatics boundary value problem that change both the potential and the magnetic field. To solve the new problem rigorously requires starting with Laplace's equation. The systematic errors of this type that we will discuss are the bounded bath, the presence of a nerve bundle surrounding the axon, and the presence of the insulated toroid in the external medium.

Bounded External Bath. The volume conductor model, as originally derived, assumes that the axon lies in an unbounded external medium. Experiments, however, must be performed in a bath of finite size. Our next goal is to calculate the change of the magnetic field due to the walls of the bath.

We consider a single insulating plane surface parallel to the axon. The potential and its resulting magnetic field can calculated exactly (Roth, B., and J. Wikwso, manuscript in preparation). Qualitatively the plane surface can be replaced by an image axon, as in Fig. 7. The image axon does not thread the toroid, and will therefore only contribute to the return current, making the total magnetic field both smaller and wider. The size of this effect is determined by s, the distance between the axon and its image. As s becomes larger than the spatial length of the depolarization phase of the action potential, the image axon's contribution to the return current becomes negligible. Fig. 8 shows the predicted magnetic field for various values of s. For s = 5.0 mm (2.5 mm from the axon to the edge of the bath), the magnetic field will differ in amplitude from its $s = \infty$ value by <2%.

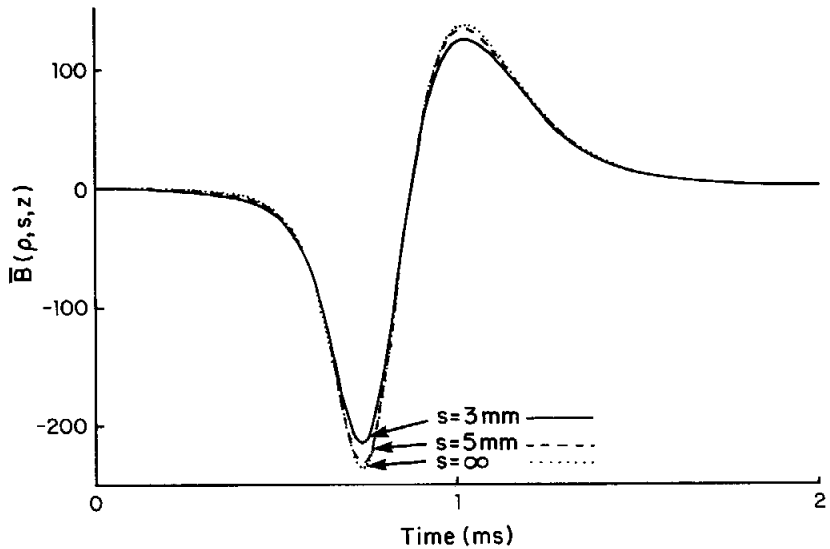

FIGURE 8 The magnetic field corrected for the axon being next to a plane surface. The distance between the axon and its image, s, is equal to ∞, 5, and 3 mm for the three traces. $a = 0.107$ mm, $\sigma_i = 1.70\ \Omega^{-1}\ m^{-1}$, $\sigma_e = 2.06\ \Omega^{-1}\ m^{-1}$, $\rho = 1.48$ mm, $u = 16.5$ m/s.

In this experiment the nerve was supported in the bath by several threads, so that the fluid could extend both above and below the toroid. The bath was ~40 mm wide, 100 mm long, and extended 10 mm below and 6 mm above the axon. If we consider only the surface closest to the axon, we calculate that the effect of the bath is to decrease the magnetic field by ~0.1%. By raising and lowering the bath level, we found experimentally that for $s > 4$ mm there was no observable change in the magnetic field. We therefore consider the systematic error introduced by the bath surfaces to be negligible compared with other possible errors in the experiment.

Anisotropic Nerve Bundle. We have been comparing our measured magnetic field to results predicted by a model of an isolated axon. However, the medial giant axon of the crayfish lies in a nerve bundle. We can extend the volume conductor model to account for the presence of the nerve bundle, but our ability to make reliable calculations is hampered by our lack of knowledge of the bundle conductivity. We have some experimental evidence suggesting that the conductivity is such that the bundle does not significantly alter the magnetic field from that which would be produced by an isolated axon. Nevertheless, determining the effect of the nerve bundle remains one of the most challenging questions we face in interpreting our biomagnetic measurements.

When studying the external potential, Stegeman et al. (10) modeled the nerve trunk as an axon surrounded by an anisotropic bundle. We have developed a similar model to calculate the magnetic field, but have included a third layer representing a sheath enclosing the entire bundle and have allowed the nerve axon to lie away from the center of the bundle. The geometry and the definition of symbols are shown in Fig. 9. The symbols σ_b^z and σ_b^ρ represent the axial and radial conductivities in the bundle, unequal in the anisotropic case. Like the correction for the bath discussed above, the potential and the magnetic field can both be calculated analytically (11).

Because we do not have good values for t, σ_s, σ_b^z, σ_b^ρ, or the thickness of the sheath, it is difficult to compare theory and experiment quantitatively. We can make some qualitative conclusions if we assume that $\sigma_b^\rho/\sigma_b^z < 1$ and $\sigma_s < \sigma_e$. Then the model predicts that both the external potential and the magnetic field will be smaller and wider than the field of an isolated axon, the amount of widening depending on the conductivities. The effect will be largest when the axon lies at the center of the nerve bundle. As the axon is moved away from the center, the effect of the bundle on the magnetic field will be diminished. For a more quantitative estimate of this effect we shall make some reasonable estimates of the unknown parameters. We let $\sigma_b^z = 2.0\ \Omega^{-1}\ m^{-1}$ and $\sigma_b^\rho = 0.2\ \Omega^{-1}\ m^{-1}$, so that $\sigma_b^\rho/\sigma_b^z = 0.1$. We assume the sheath has a thickness of 10 μm, and a conductivity of $0.2\ \Omega^{-1}\ m^{-1}$. We estimate that the bundle radius, b, is 0.625 mm,[2] implying $c = 0.635$ mm. In the crayfish, the giant axons are near the edge of the bundle, so we let $t = 0.450$ mm. The magnetic field calculated using these parameters is shown in Fig. 10, along with the calculated field produced by an isolated axon.

[2]The high precision is necessary to make the geometry self-consistent. It in no way reflects the accuracy of our values.

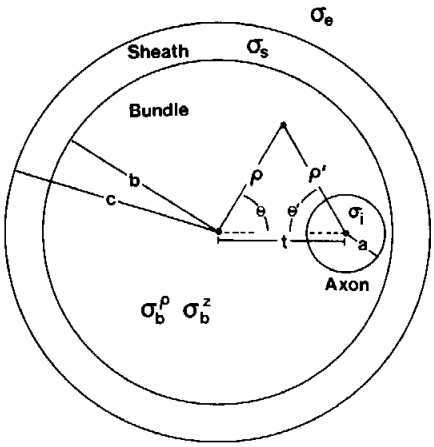

FIGURE 9 Geometry for an axon in an anisotropic, sheathed nerve bundle. σ_s is the conductivity of the sheath. σ_b^z and σ_b^ρ are the axial and radial conductivities of the bundle. b and c are the inner and outer radii of the sheath. The distance from the center of the bundle to the center of the axon is labeled t.

When comparing the predictions of the bundle model with experiment, any change in the size of the magnetic field will be masked by our uncertainty of a and σ_i. We therefore must base all our conclusions on changes in the shape of the signal. The bundle model predicts that the measured magnetic signal should be wider than the prediction for an isolated axon. In all data taken in this study we observed no such widening. In fact, as seen in Fig. 4, we consistently found the measured magnetic field to be slightly narrower than the volume conductor model predicted. We conclude that the conductivities of the bundle and sheath must not differ substantially from the conductivity of the bath, so that they will have little effect on the magnetic field. For this reason, we believe we can use our model of an isolated axon to investigate a crayfish axon in a nerve bundle.

Presence of the Toroid. Another important inhomogeneity in the external conductivity is the toroid. Current cannot flow through the epoxy layer encapsulating the toroid and instead must flow either around the outside of the toroid or through the hole in its center. Since the toroid is quite close to the axon, we might expect a large redistribution of the current density and possibly a significant change in the magnetic field.

The natural way to account for the presence of the toroid would be to again solve Laplace's equation, including the additional boundary condition that the normal component of the current density on the toroid surface is zero. Unfortunately this electrostatics problem apparently does not have an analytic solution, so we are forced to adopt a numerical method. We have chosen an iterative procedure, like that used by Gelernter and Swihart to calculate the potential on the body surface due to electrical activity within the heart (12).

To meet the additional boundary condition on the toroid surface we place a charge density on the toroid that will just cancel the normal component of the current density that would exist if the toroid were not present. We account for the interaction of these charges with each other by iteration, finally obtaining a solution to Laplace's equation that meets all the prescribed boundary conditions. Once

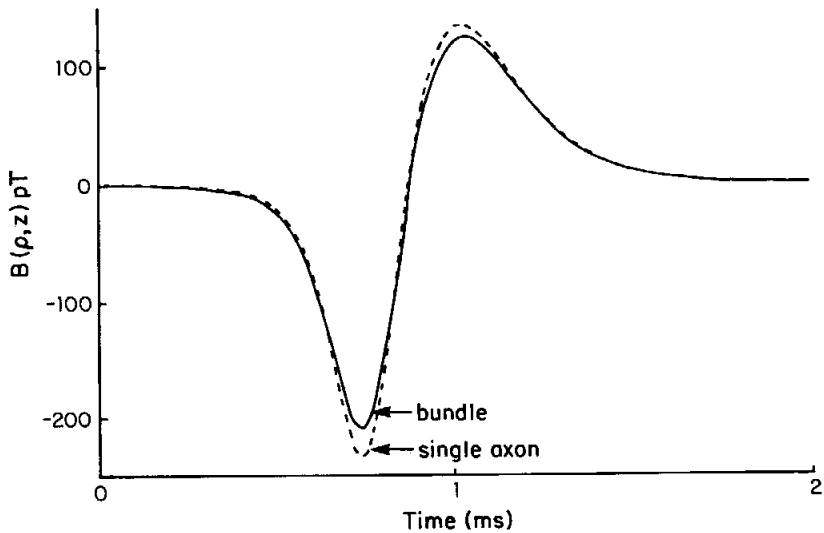

FIGURE 10 The magnetic field of an axon off-axis in a sheathed, anisotropic nerve bundle. $a = 0.107$ mm, $\sigma_i = 1.70\ \Omega^{-1}\ m^{-1}$, $\sigma_e = 2.06\ \Omega^{-1}\ m^{-1}$, $\rho = 1.48$ mm, $u = 16.5\ m/s^{-1}$, $\sigma_s = 0.2\ \Omega^{-1}\ m^{-1}$, $\sigma_b^z = 2.0\ \Omega^{-1}\ m^{-1}$, $\sigma_b^\rho = 0.2\ \Omega^{-1}\ m^{-1}$, $b = 0.625$ mm, $c = 0.635$ mm, $t = 0.45$ mm.

this potential is found, we can immediately calculate the current density and the magnetic field (Roth, B., and J. Wikswo, manuscript in preparation).

The results of these calculations indicate that the effect of the toroid on the magnetic field depends strongly on the dimensions of its epoxy coating (Fig. 2). Most of the current in the bath flows around toroids having inner and outer radii that are small compared with the depolarization width of the action potential. This means there will be less return current than if the toroid were absent, so the magnetic field gets larger and narrower. If the toroid is wide, it will appear as a tube encircling the axon. The current density will be forced to flow through the toroid, thus increasing the return current and making the magnetic field smaller and wider. Toroids of the geometry used in this experiment have an intermediate effect. The current density redistributes itself so that there is little change in the return current or the magnetic field. Calculation shows that the peak-to-peak amplitude of the magnetic field increases by ~1%, and the FWHM narrows by <1%.

Other Systematic Errors

There is a final class of systematic errors in this experiment that are harder to quantify. These often deal with deviations of the axon from our model assumptions. For instance, the axon membrane was observed not to form a perfect cylinder, but to have a radius that varied by 10% over distances <1 mm. Since the magnetic field depends strongly on the axon cross-sectional area, and since a change in the area could lead to corresponding changes in the conduction velocity and action potential shape, at some point our model will cease to describe the axon accurately. However, the magnetic signal was not observed to vary when the axial position of the toroid was changed by a few millimeters near the microelectrode penetration. This is because the magnetic field represents a weighted average of the current density over more than a millimeter along the axon length, so that local random fluctuations in the geometry are averaged out. We therefore consider small deviations from cylindrical geometry to have a minor effect on the magnetic field.

Since the active axon was not completely isolated from the nerve bundle, there remains the possibility of more than one axon contributing to the signal. The complete dissection of a single axon was attempted several times, but at least a few millimeters of the axon would have to be isolated and the trauma of the dissection invariably killed or severely damaged it. However, we are confident that only one of the giant axons was firing. Only one branch of the esophogeal connective was stimulated and changes in stimulus strength, duration, and polarity always gave the same all-or-none response. We were able to determine which axon was producing this signal by observing under a microscope which of the four giant axons had been penetrated by the microelectrode. If there are small axons that fire if and only if a medial giant axon also fires (13) their contribution may also be present in the magnetic signal, but because of their much smaller radius, their contribution would be minimal. For these reasons, and because of the good agreement between theory and experiment, we conclude that both the magnetic and electric signals are due only to a single medial giant axon.

The volume conductor model assumes that the electric and magnetic fields are quasistationary. One aspect of this assumption has been investigated when we showed that the inductive contribution to the electric field is negligible. Plonsey and Heppner (8) made a careful analysis of quasistationarity and conclude that deviations from this assumption will first appear as capacitive effects. It is interesting to compare the error made in ignoring capacitive effects to other errors we have considered.

Capacitive effects are negligible if

$$\frac{\omega\epsilon_0\kappa}{\sigma} \ll 1, \tag{9}$$

where $\epsilon_0 = 8.9 \times 10^{-12}\ \mathrm{s\,\Omega^{-1}\,m^{-1}}$ is the permittivity of free space, ω is an angular frequency, and κ and σ are the dielectric constant and the conductivity of the conducting medium. Angular frequencies from 0 to $\sim 6 \times 10^4$ radians $\mathrm{s^{-1}}$ contribute to the action potential, corresponding to frequencies from 0 to 10 kHz. To evaluate the left-hand side of Eq. 9, we must know σ and κ for the crayfish nerve axoplasm. We will use $\sigma = 1\ \Omega^{-1}\,\mathrm{m}^{-1}$ as a lower bound for the conductivity. The dielectric constant should be similar to that of water, $\kappa = 80$. We then find that $\omega\epsilon_0\kappa/\sigma$ has its largest value when ω is large, and that for $\omega = 6 \times 10^4$ radians $\mathrm{s^{-1}}$ (10 kHz)

$$\frac{\omega\epsilon_0\kappa}{\sigma} \approx \frac{(6 \times 10^4\ \text{radians s}^{-1})(8.9 \times 10^{-12}\ \mathrm{s\,\Omega^{-1}m^{-1}})(80)}{(1\ \Omega^{-1}\mathrm{m}^{-1})}$$

$$\approx 4 \times 10^{-5}. \tag{10}$$

Capacitive effects will therefore be on the order of 0.01% or less. Even if we have incorrectly estimated κ by as much as an order of magnitude by ignoring any contribution from structure inside the axon, capacitive effects should still be negligible in this experiment.

As discussed in reference 1, there is an error introduced by considering the potential measured by the microelectrode to be the transmembrane potential instead of the potential difference between the inside of the axon and a distant ground. According to the results of our single axon model, the transmembrane potential is slightly larger and narrower than the potential measured by the microelectrode. There is a corresponding 1% error in the peak-to-peak amplitude of the magnetic field calculated from the microelectrode potential and less than a 1% narrowing of the FWHM.

A final source of error is the possibility that penetration by the microelectrode may damage the axon. Presumably this would be local damage and therefore effect primarily the microelectrode signal. Transmembrane potential sig-

nals with unusually small amplitudes and long repolarization phases, or that varied with time while the magnetic signal stayed constant, were attributed to poor microelectrode penetration and were not considered in the analysis of the data. We do not know if damage due to the microelectrode is absent or just minimized in our best penetrations. This source of systematic error of course disappears if magnetic measurements alone are used to study the nerve.

A list summarizing the possible sources of error in this experiment follows this section. The largest uncertainty is in our knowledge of the axon radius and the internal conductivity, or the internal resistance per unit length r_i. If we use the data to determine r_i, we eliminate the dominant source of error in the experiment. By computing the square root of the sum of the squares of the remaining uncertainties, we find that the uncertainty in the amplitude of the magnetic field, and therefore the uncertainty in r_i, is 10%, while the uncertainty in the FWHM of the magnetic signal is 4%. Of the sources of error that we were not able to quantify, the most significant is probably the presence of the nerve bundle, followed by local damage due to the microelectrode and the variation of the conduction velocity over the length of the axon between the toroids. We note that the quoted uncertainty in r_i does not include any contribution from these last three sources of error because we were not able to quantify their effect.

The overall shape of the magnetic signal, in particular the asymmetry of the depolarization and repolarization peaks, agrees quite well between theory and experiment. However, the 12% difference of the FWHM between the measured and calculated magnetic signals has not yet been entirely explained. Evidence that the source of this discrepancy may lie in the electric, not the magnetic, data is found by examining the external potential.

Summary of Error Sources

The two percentages given represent the uncertainty that the source of error introduces in the peak-to-peak amplitude and the width (FWHM of the depolarization phase) of the magnetic field.

Major Sources of Error.

□ UNCERTAINTY IN THE INTERNAL CONDUCTIVITY 50%, <1%. This value was taken from the literature. The magnetic field, as calculated from the transmembrane potential, is proportional to σ_i.

□ UNCERTAINTY IN THE AXON RADIUS 20%, <1%. The error arose from a 10% uncertainty in the measurement of the axon radius, a. The magnetic field, as calculated from the transmembrane potential, is proportional to a^2.

Small Sources of Error.

□ UNCERTAINTY IN THE EFFECTIVE RADIUS OF THE TOROID 8%, 2%. The error is due to a 5% uncertainty in the toroid core dimensions. This is the largest source of error contributing to the value of r_i predicted by the data.

□ UNCERTAINTY IN THE CONDUCTION VELOCITY 4%, 3%. The origin of the error is a 10% uncertainty in the measured conduction velocity. Of the five volume conductor model parameters, the shape of the calculated magnetic field is most sensitive to the conduction velocity.

□ AXON OFF-AXIS IN THE TOROID 2%, <1%. Makes the measured magnetic signal larger, narrower.

□ INACCURATE FREQUENCY COMPENSATION 2%, 2%. Changes both the size and shape of the measured magnetic field and the measured transmembrane potential.

□ REDISTRIBUTION OF THE CURRENT DENSITY DUE TO THE TOROID 1%, <1%. For our toroid, makes the measured magnetic signal larger and narrower.

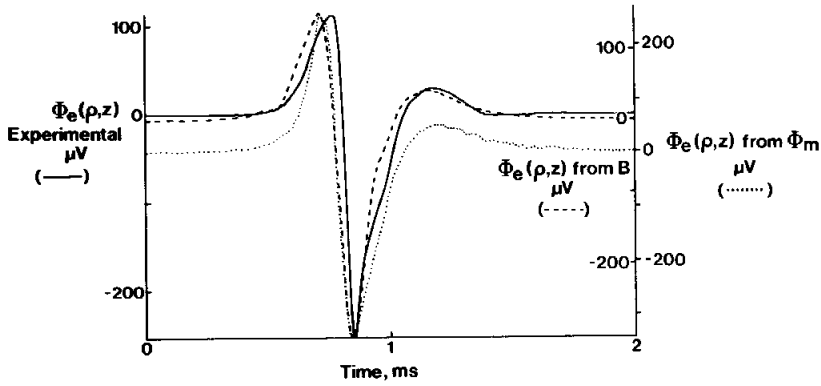

FIGURE 11 The external potential calculated from the transmembrane potential (dotted), calculated from the magnetic field (dashed), and measured (solid).

□ CONSIDERING THE MICROELECTRODE SIGNAL AS A DIRECT MEASUREMENT OF THE TRANSMEMBRANE POTENTIAL 1%, <1%. Makes the calculated magnetic field larger and narrower.

Negligible Sources of Error.

□ UNCERTAINTY IN THE EXTERNAL CONDUCTIVITY 0.1%, 0.1%.

□ EFFECT DUE TO THE BOUNDARIES OF THE BATH 0.1%, 0.1%. Makes the measured magnetic field smaller and narrower.

□ CAPACITIVE EFFECTS $<10^{-2}\%$, $<10^{-2}\%$.

□ INDUCTIVE EFFECTS $<10^{-5}\%$, $<10^{-5}\%$.

Sources of Error that We Believe Are Small but whose Effects Are Difficult to Quantify.

□ THE PRESENCE OF THE NERVE BUNDLE AROUND THE AXON ??%. Makes the measured magnetic signal smaller and wider. A knowledge of the bundle conductivity is required to quantify this effect.

□ LOCAL DAMAGE BY THE MICROELECTRODE ??%. Changes the measured transmembrane potential.

□ VARIATION OF THE AXON RADIUS AND CONDUCTION VELOCITY ??%.

□ AXON NOT PERPENDICULAR TO THE PLANE OF THE TOROID ??%. Must consider boundary conditions for the magnetic field at the ferrite surface.

□ MORE THAN ONE AXON CONTRIBUTING TO THE SIGNAL ??%.

EXTERNAL POTENTIAL

An additional observation that sheds some light on the relationship between the magnetic field, B, and the transmembrane potential, Φ_m, is their relationship to the measured external electric signal, Φ_e. Using the volume conductor model (1), we can calculate Φ_e from both the magnetic field and the transmembrane potential. The results of these calculations and the measured Φ_e are shown in Fig. 11. Again, the vertical scales are adjusted so that the signals all have the same peak-to-peak amplitude. The major difference between the shapes of the signals is the relative size of the three phases. In this respect, the external potential calculated from the magnetic field matches the measured external potential much better than the external potential calculated from the transmembrane potential. Thus a third, independent measurement agrees better with the magnetic than the transmembrane potential data. The difference seems to be in the second phase of the signal, which is smaller for Φ_e calculated from the transmembrane potential. Since Φ_e is qualitatively the second derivative of Φ_m, this means that the curvature at the maximum of the microelectrode signal is not as large as the other two signals predict, i.e., Φ_m really has a narrower peak than the transmembrane potential data suggests. The effect may be due to the limited bandwidth of the microelectrode, which could not be totally compensated for by negative capacitance, or could be due to membrane damage from the microelectrode penetration. If this hypothesis is correct, then we are led to the conclusion that in this experiment magnetic techniques may provide a better measurement of the shape of the transmembrane action potential than do microelectrodes!

Since Φ_e and B are both proportional to r_i, we expect that the uncertainty in the axon resistance will play no role in the comparison of the relative amplitudes of the external potential calculated from the magnetic field and the measured external potential. The two signals have peak-to-peak amplitudes that differ by 21%, the discrepancy probably being due to the uncertainty in the location of the field point for Φ_e. The difference in the peak-to-peak amplitude of the Φ_e data and the external potential calculated from the transmembrane potential is 46%.

The analysis of the external potential completes our comparison of the volume conductor model predictions to experimental data. Although there are some small discrepancies still remaining, we believe that the results of this comparison verify the usefulness of this model, and that this paper, along with reference 1, provide a complete and accurate description of the magnetic field of a single axon. To our knowledge, we have considered every source of error that could enter our data, not only for the purpose of placing error bounds on our value for r_i, but more importantly to determine the accuracy that is obtainable with our relatively new biomagnetic technique. In the last section of this paper we compare the use of this magnetic technique to other experimental methods commonly used in the study of nerve axons.

COMPARISON OF BIOMAGNETIC AND BIOELECTRIC MEASUREMENTS

To conclude our discussion, we shall compare the relative merits of measuring the extracellular magnetic field to the standard electrophysiological measurements of the transmembrane and external potentials. Any of these three quantities can be measured and therefore serve as the basis for a study of nerve behavior. By surveying the experimental and computational advantages and disadvantages associated with each field, we hope to make clear which is most appropriate for any particular investigation.

The relationships between the magnetic field, B, the transmembrane potential, Φ_m, and the external potential, Φ_e, are summarized schematically by the triangle in Fig.

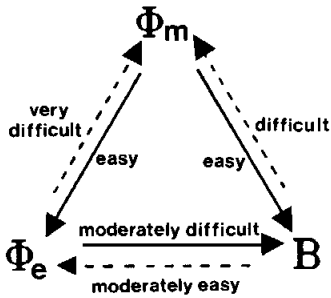

FIGURE 12 A schematic drawing demonstrating the relationship between the transmembrane potential Φ_m, the magnetic field B, and the external potential Φ_e. A solid line indicates a forward calculation, while a dashed line indicates an inverse calculation.

12. Each vertex of the triangle represents a measurable bioelectric or biomagnetic field, and each arrow directed from one of the fields to another represents a possible calculation with the volume conductor model. There are two types of arrows, solid and dashed, representing forward and inverse calculations, respectively. By a forward calculation we mean a computation in which the field point of the calculated signal, ρ_{calc}, is farther from the axon than the field point of the measured signal, ρ_{meas}, or $\rho_{calc} > \rho_{meas}$. Conversely, an inverse calculation is one in which $\rho_{calc} < \rho_{meas}$. All else being equal, an inverse calculation will always be more difficult than a forward calculation because the inverse calculation has the property of exaggerating the high frequency noise present in the measured data. This is most easily understood by inspecting the filter functions of the volume conductor model (see Appendix A). In a forward calculation the filter function goes to zero as the spatial frequency k becomes large, so that the calculated signal contains very little of the high frequency noise that was present in the data. The filter function for an inverse problem goes to infinity at large k, implying that high frequency noise in the measured signal will be amplified in the calculated field. From a computational point of view, it is advantageous to make forward calculations. Unfortunately, it is the inverse calculations that are usually of most interest. Calculation of the transmembrane potential from either the magnetic field or the external potential is an inverse calculation and, in our experiment, the calculation of Φ_e from B is also.

The difficulty of each computation is written next to its corresponding arrow in Fig. 12. As expected, the inverse calculation of computing Φ_m from either B or Φ_e is more difficult than its forward counterpart. However, the inverse calculation of Φ_e from B is described as being easier than the corresponding forward calculation. Clearly there must be another factor in determining which calculation can be performed with least difficulty. We found in our study that calculations that qualitatively represent an integration are more difficult than those that represent a differentiation. Again, we can see why this is true by looking at the filter functions. Those filter functions that correspond to integrations have the property of rising to infinity as the spatial frequency goes to zero. So, just as an inverse calculation tends to exaggerate high frequency noise in the data, an integration will tend to exaggerate low frequency noise. Calculating Φ_m from B and B from Φ_e both represent integrations and therefore are difficult to perform accurately. Calculating Φ_m from Φ_e requires two integrations, making this computation yet harder to carry out.

These ideas are summarized in Table I, in which each row corresponds to one of the six possible computations. Those computations representing integrations have an asterisk in the column labeled "difficulty at low frequencies," while those representing inverse calculations have an asterisk in the column labeled "difficulty at high frequencies." The Φ_e to Φ_m calculation has two asterisks in the first column because it requires two integrations. The difficulty of each calculation can be estimated by the number of asterisks in that row. The rows corresponding to the calculations of either B or Φ_e from Φ_m contain no asterisks, and these calculations are very easy. The rows associated with the calculations of B from Φ_e or Φ_e from B each have one asterisk, and are of moderate difficulty. We found that the difficulties associated with integrations were slightly more severe than the difficulties associated with inverse calculations, so that calculating Φ_e from B is moderately easy, while calculating B from Φ_e is moderately hard. The row containing the calculation of Φ_m from B (Fig. 5) has asterisks in both columns, so it is a quite difficult calculation to perform and requires very clean magnetic data. However, the calculation of Φ_m from Φ_e has three asterisks in its row, so it is extremely difficult. This computation places such demands on the quality of the Φ_e data that reliable calculations of Φ_m from Φ_e are almost impossible. It is unfortunate that the two calculations of most interest, calculating Φ_m from measurements of either B or Φ_e made outside the axon, are the two most difficult to perform. However, a calculation of the transmembrane potential is

TABLE I
SUMMARY OF CALCULATIONS SHOWN IN FIG. 12

Calculation	Difficulty at low frequencies	Difficulty at high frequencies	Calculated field is proportional to:
$\Phi_m \rightarrow B$			$\sigma_i a^2$
$\Phi_m \rightarrow \Phi_e$			$\frac{\sigma_i a^2}{\sigma_e}$
$B \rightarrow \Phi_e$		*	$\frac{1}{\sigma_e}$
$\Phi_e \rightarrow B$	*		σ_e
$B \rightarrow \Phi_m$	*	*	$\frac{1}{\sigma_i a^2}$
$\Phi_e \rightarrow \Phi_m$	**	*	$\frac{\sigma_e}{\sigma_i a^2}$

less difficult when based on the magnetic field than when based on the external potential. This fact represents a major computational advantage of extracellular magnetic measurements over extracellular electric measurements.

Table I also indicates which parameters in the volume conductor model are most important in determining the amplitude of the fields; the calculated signal is proportional to the factor in column 3. Determination of the axon internal resistance, $r_i = 1/(\pi\ a^2\sigma_i)$, is often of interest. Inspection of Table I shows that this quantity can be obtained most directly by measuring both Φ_m and B and fitting the theory and experiment to evaluate r_i.

Fig. 13 contains plots of the three measured and the six calculated fields. Forward calculations are marked by an arrow containing a small f, while inverse calculations are designated by an i. Apparently there is some low frequency noise in the external electric data because the magnetic field calculated from it has an offset occurring between the beginning and end of the signal. This is even more pronounced in the transmembrane potential calculated from the external potential. Note that the transmembrane and external potentials as calculated from the magnetic field (panels *b* and *h*) more closely resemble the corresponding measured signals (panels *a* and *i*) than do the potentials calculated from the electric data (panels *c* and *g*). This may in part reflect the relative experience of the investigators in using magnetic and external electric techniques, but the difference, particularly in panel *c*, is also due to factors summarized in Table I, which imply that the calculation of the transmembrane potential from the external potential is extremely difficult.

If only computational factors are considered, one would always choose to measure the transmembrane potential and compute the other fields from it. However, experimental factors often make the direct measurement of Φ_m with microelectrodes undesirable. The primary disadvantages of microelectrode measurements are that they require penetration of the axon and that they may not provide a stable signal over several hours. Measurements of the magnetic field or the external potential are both noninvasive techniques and share the common attributes that they do not puncture the axon and provide stable and reproducible results. They also have similar signal-to-noise ratios (both of which are lower than the signal-to-noise ratio of microelectrode measurements), and both fall off rapidly away from the axon, so they require the field point to be known precisely. Both the toroid and external microelectrodes exhibit a decreased signal-to-noise ratio at low frequencies and the toroid is insensitive to steady currents. A toroid has the advantage that its dimensions are fixed and can be measured before an experiment, while a tungsten electrode has to be carefully located with a micropositioner and may move while taking data. The electric potential measurement that would most closely resemble our magnetic technique would be to measure the external potential using a loop electrode encircling the

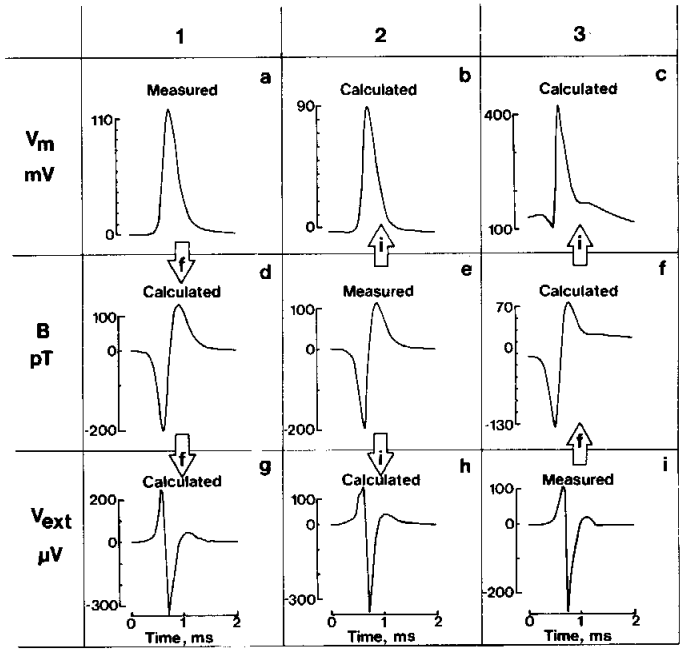

FIGURE 13 *a*, *e*, and *i* are plots of the measured transmembrane potential, magnetic field, and external potential. The other six panels contain fields calculated using the volume conductor model. An arrow containing a small *f* indicates a forward calculation, while a small *i* indicates an inverse calculation.

nerve. However, magnetic techniques would still have the additional practical advantage that the ferrite core is encapsulated in a layer of insulation so that there is no electrical connection between the toroid and the nerve, as there must be with a metal electrode. Also, the toroids are more robust and less easily damaged than metal electrodes. Finally, magnetic measurements with toroids have been found to be less sensitive to stimulus artifact.

At present, magnetic measurements have the disadvantage over electric techniques in that they require the complete dissection of at least one end of the axon so that it may be threaded through the toroid. However, openable clip-on toroids are now being developed that will eliminate this requirement (14; Henry, P., F. Gielen, and J. Wikswo, manuscript in preparation). Also, magnetic techniques cannot yet match external electric or microelectrode measurements for spatial resolution. The development of smaller, thinner toroids should be possible, and will increase the ability of magnetic techniques to look at higher frequency and more slowly propagating events.

CONCLUSION

The results of this paper indicate that the volume conductor model allows the magnetic field of a nerve axon to be accurately calculated from the transmembrane potential, provided the resistance of the axon is known. Perhaps more importantly, this procedure can be inverted to calculate the transmembrane potential from the measured magnetic field without penetrating the axon. If the intracellular current is of interest, the magnetic measurements provide this information directly. Thus, if the resistance of the axon is unknown, it can be obtained by measuring both the magnetic field and the transmembrane potential, yielding values of r_i more precise than obtained by subthreshold electrotonic measurements. After considering all sources of error that could enter our measurements, we believe that the magnetic field can be measured with sufficient ease and accuracy for magnetic techniques to be viewed as a tool that is comparable and complementary to microelectrodes and external potential measurements for use in the study of electrically active tissue.

APPENDIX A

A nerve axon can be modeled as a cylindrical, infinitely long membrane of radius a separating the intracellular space with conductivity σ_i from the extracellular space with conductivity σ_e (Fig. 14). An action potential propagating down the axon with conduction velocity u is described by the transmembrane potential $\Phi_m(z)$. Given this transmembrane potential the potential inside and outside the axon is found by solving Laplace's equation. The results are

$$\phi_i(\rho, k) = \frac{I_0(|k|\rho)}{\beta(|k|a)\, I_0(|k|a)}\,\phi_m(k), \tag{A1}$$

$$\phi_e(\rho, k) = \frac{K_0(|k|\rho)}{\alpha(|k|a)\, K_0(|k|a)}\,\phi_m(k), \tag{A2}$$

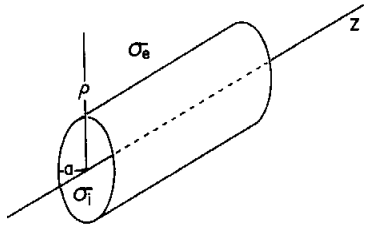

FIGURE 14 The geometry of a nerve axon.

where α and β are defined as

$$\alpha(|k|a) = -(1 + \gamma(|k|a)), \tag{A3}$$

$$\beta(|k|a) = 1 + \frac{1}{\gamma(|k|a)}, \tag{A4}$$

with γ given by

$$\gamma(|k|a) = \frac{\sigma_e K_1(|k|a) I_0(|k|a)}{\sigma_i K_0(|k|a) I_1(|k|a)}. \tag{A5}$$

I_0, I_1, K_0, and K_1 are modified Bessel functions, $\phi_m(k)$ is the Fourier transform of the transmembrane potential, defined as

$$\phi_m(k) = \int_{-\infty}^{\infty} \Phi_m(z) e^{+ikz} dz, \tag{A6}$$

k is the spatial frequency, and $\phi_i(\rho, k)$ and $\phi_e(\rho, k)$ are the Fourier transforms of the internal and external potentials.

We have extended this calculation to include the magnetic field (1). Ampere's law states that the line integral of the magnetic field around a closed path is proportional to the net current through that path, $I_{enclosed}$

$$\oint_c \mathbf{B} \cdot d\mathbf{l} = \mu_0 I_{enclosed}. \tag{A7}$$

For cylindrically symmetric current distributions, it is convenient to take the line integral path as a circle of radius ρ, centered on and perpendicular to the axis of the nerve. Then Ampere's law reduces to

$$B = \frac{\mu_0}{4\pi\rho} I_{enclosed}. \tag{A8}$$

To find $I_{enclosed}$ we make use of Ohm's law and differentiate the Fourier transforms of the potentials given in Eqs. A1 and A2 to find the Fourier transforms of the axial current density

$$J_i^z(\rho, k) = i\sigma_i k \phi_i(\rho, k), \tag{A9}$$

$$J_e^z(\rho, k) = i\sigma_e k \phi_e(\rho, k). \tag{A10}$$

Next we must integrate the current density over the area bounded by our line integral path. The radial integration makes use of the Bessel function relationships

$$\int I_0(x) x dx = x I_1(x), \tag{A11}$$

$$\int K_0(x) x dx = -x K_1(x). \tag{A12}$$

After performing the integration to find $I_{enclosed}$, we use Eq. A8 to find the Fourier transform of the magnetic field

$$\mathcal{B}(\rho, k) = \frac{i\mu_0 k}{\rho |k|}\left\{\frac{\sigma_i a I_1(|k|a)}{\beta(|k|a) I_0(|k|a)} + \frac{\sigma_e}{\alpha(|k|a)\, K_0(|k|a)} \cdot [aK_1(|k|a) - \rho K_1(|k|\rho)]\right\}\phi_m(k). \tag{A13}$$

This is our final result, the Fourier transform of the magnetic field written in terms of the Fourier transform of the transmembrane potential.

Eq. A13 determines one Fourier transform by multiplying another Fourier transform by a function of the frequency (k). This function can thus be thought of as a filter applied to the transmembrane potential to obtain the magnetic field. We call this function the filter function relating the two fields. Note that if Eq. A13 is divided on both sides by the filter function, then we have a relationship that represents the solution to the inverse problem of calculating ϕ_m from $\mathcal{B}$.

APPENDIX B

The volume conductor model can be extended to calculate the change in the magnetic field due to an axon being off-axis in the toroid.

Fig. 15 shows the geometry used to investigate the magnetic field of an axon off-axis a distance ℓ from the center of the toroid. Because the measured magnetic field depends only on the net current threading the toroid, the magnetic field due to the total internal current B_{itot} is unchanged as the axon is moved off the z-axis. We can use Ampere's law to calculate the magnetic field due to the return current. The Fourier transform of the external potential, $\phi_e(k)$, can be written in terms of $\phi_m(k)$, the Fourier transform of the transmembrane potential and modified Bessel functions (see Appendix A)

$$\phi_e(\rho_2, k) = \frac{K_0(|k|\rho_2)}{\alpha(|k|a)K_0(|k|a)}\phi_m(k), \qquad \text{(B1)}$$

where

$$\rho_2^2 = \rho^2 + \ell^2 - 2\rho\ell\cos\theta. \qquad \text{(B2)}$$

By differentiation of the external potential with respect to z, and by using the Bessel function relations

$$K_0(|k|\sqrt{\rho^2 + \ell^2 - 2\rho\ell\cos\theta}) = K_0(|k|\ell)I_0(|k|\rho) + 2\sum_{m=1}^{\infty}\cos m\theta\, K_m(|k|\ell)I_m(|k|\rho), \qquad \rho < \ell \qquad \text{(B3)}$$

$$K_0(|k|\sqrt{\rho^2 + \ell^2 - 2\rho\ell\cos\theta}) = I_0(|k|\ell)K_0(|k|\rho) + 2\sum_{m=1}^{\infty}\cos m\theta\, I_m(|k|\ell)K_m(|k|\rho), \qquad \rho > \ell \qquad \text{(B4)}$$

we can calculate J_e^z, the external axial current density, as a function of ρ and θ.

From Ampere's law we get $\overline{\mathcal{B}}_{ret}$, the transform of the magnetic field due to the return current averaged over all angles, by integrating J_e^z over the area between the axon and the field point radius

$$\overline{\mathcal{B}}_{ret}(\rho, \ell, k) = \frac{\mu_0}{2\pi\rho}\int_0^{2\pi}\int_0^{\rho} J_e^z(\rho, \theta, \ell, k)\rho\,d\rho\,d\theta - \frac{\mu_0}{2\pi\rho}\int_0^{2\pi}\int_0^{a} J_e^z(\rho_2, k)\rho_2\,d\rho_2\,d\theta. \qquad \text{(B5)}$$

Orthogonality of the trigonometric functions insures that only the $m = 0$ terms survive the integration over θ. We then can use the Bessel function relations given in Eqs. A11 and A12 to integrate radially, which after some algebra reduces to

$$\overline{\mathcal{B}}_{ret}(\rho, \ell, k) = \frac{\mu_0 i\sigma_e k}{|k|\rho\alpha(|k|a)K_0(|k|a)} \cdot \{aK_1(|k|a) - \rho I_0(|k|\ell)K_1(|k|\rho)\}\phi_m(k). \qquad \text{(B6)}$$

By adding $\overline{\mathcal{B}}_{ret}$ to the magnetic field due to the total internal current $\mathcal{B}_{itot}$, and by using a relation derived from the Wronskian, we find that the Fourier transform of the total magnetic field due to an axon a distance ℓ off-axis in a toroid can be written

$$\overline{\mathcal{B}}(\rho, \ell, k) = I_0(|k|\ell)\mathcal{B}(\rho, k), \qquad \text{(B7)}$$

where $\mathcal{B}(\rho,k)$ is the Fourier transform of the total magnetic field when the axon is at the center of the toroid, given in Appendix A by Eq. A13.[3] When ℓ goes to zero, $I_0(|k|\ell)$ goes to one, recovering our original result, and for $|k|\ell << 1$ the nerve that is off-axis produces a small change in the magnetic field. This condition is equivalent to requiring that ℓ be much smaller than the spatial width of the depolarization phase of the action potential.

We note that the simple form of the correction in Eq. B7 is entirely due to our toroid geometry. If our toroids were not cylindrically symmetric, the measured magnetic field would be much harder to calculate.

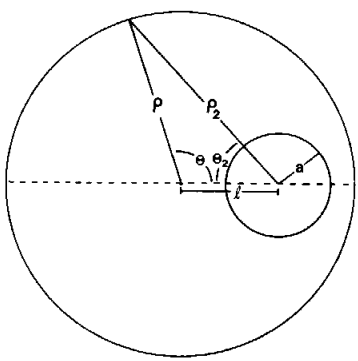

FIGURE 15 The geometry of an axon off-axis in a toroid.

APPENDIX C

The magnetic field averaged over the toroid cross section can be calculated using the volume conductor model. The equation relating the Fourier transform of the magnetic field to the Fourier transform of the transmembrane potential, given by Eq. 36 in reference 1, is[4]

$$\mathcal{B}(\rho, k) = i\mu_0 akI_1(|k|a)K_1(|k|\rho) \cdot \left\{\frac{\sigma_i}{\beta(|k|a)} - \frac{\sigma_e}{\alpha(|k|a)}\right\}\phi_m(k). \qquad \text{(C1)}$$

Using the Bessel function relationship

$$\int K_1(x)dx = -K_0(x) \qquad \text{(C2)}$$

we can integrate the magnetic field over the toroid dimensions to yield $\mathcal{B}(c, d, e, k)$, the transform of the magnetic field averaged over the toroid

[3] In reference 1, $\mathcal{B}_{itot}$ is defined by Eq. 43, $\mathcal{B}(\rho, k)$ by Eq. 45, and the Wronskian relationship is given in Eq. 46.

[4] Eq. C1 is exactly equivalent to Eq. A13, the filter function has just been rearranged (see reference 1). We choose this form of the filter function because it shows more clearly the consequences of integrating over the cross section of the toroid.

cross section

$$\overline{\mathcal{B}}(c, d, e, k) = i\mu_0 a k I_1(|k|a)\left\{\frac{K_0(|k|c) - K_0(|k|d)}{|k|(d-c)}\right\}\left\{\frac{\sin\frac{ke}{2}}{\frac{ke}{2}}\right\}\times\left\{\frac{\sigma_i}{\beta(|k|a)} - \frac{\sigma_e}{\alpha(|k|a)}\right\}\phi_m(k), \quad \text{(C3)}$$

where c is the core inner diameter, d the outer diameter, and e the width (Fig. 2). The factor containing $\sin(ke/2)$ represents the correction for the finite width of the toroid. It always decreases the high frequency content of the signal. The factor involving a difference of modified Bessel functions in Eq. C3 replaces $K_1(|k|\rho)$ in Eq. C1 and eliminates the need of choosing one representative value of ρ in the toroid at which to calculate the magnetic field. However, if the toroid is not too large, we can find a point in the toroid where the two correction factors in Eq. C3 nearly cancel. We then get an average field almost identical to the field calculated at one effective field point ρ_{eff}. The error introduced by using ρ_{eff} instead of Eq. C3 is <1%, smaller than our uncertainty in the toroid core dimensions.

We appreciate the aid of Shin Ho Chung in performing these experiments, the work of Ranjith Wijesinghe in calculating the effect of the nerve being off-axis in the toroid, and the comments and suggestions from Rolf Kasper, Jeffrey Wine, and Leonora Wikswo. In particular we acknowledge the contributions of James Woosley to the theoretical calculation of the magnetic field, and Frans Gielen, whose suggestions and experience with microelectrodes were invaluable.

This work was supported in part by the Office of Naval Research under contract N00014-82-K-0107, by a National Institutes of Health grant 1-R01 NS 19794-01, and by the Vanderbilt University Research Council.

Received for publication 28 September 1984 and in final form 5 February 1985.

REFERENCES

1. Woosley, J., B. Roth, and J. P. Wikswo. 1985. The magnetic field of a single axon: a volume conductor model. *Math. Biosci.* In press.
2. Wikswo, J. P., J. Barach, S. Gundersen, J. Palmer, and J. Freeman. 1983. Magnetic measurements of action currents in an isolated lobster axon. *Il Nuovo Cimento.* 2:512–516.
3. Wikswo, J. P. 1982. Improved instrumentation for measuring the magnetic field of cellular action currents. *Rev. Sci. Instrum.* 53:1846–1850.
4. Wikswo, J. P., P. Samson, and R. Giffard. 1983. A low-noise low input impedance amplifier for magnetic measurements of nerve action currents. *IEEE (Inst. Electr. Electron. Eng.) Trans. Biomed. Eng.*BME-30:215–221.
5. Wikswo, J. P., W. P. Henry, P. C. Samson, and R. P. Giffard. 1985. A current probe for measuring cellular action currents. *In* Biomagnetism Application and Theory. H. Weinberg, G. Stroink, and T. Katila, editors. Pergamon Press, New York. 83–87.
6. Hodgkin, A., and W. Rushton. 1946. The electrical constants of a crustacean nerve fibre. *Proc. R. Soc. Lond. B. Biol. Sci.* 133:444–479.
7. Watanabe, A., and H. Grundfest. 1961. Impulse propagation of the septal and commissural junctions of crayfish lateral giant axon. *J. Gen. Physiol.* 45:267–308.
8. Plonsey, R., and D. Heppner. 1967. Considerations of quasi-stationarity in electrophysiological systems. *Bull. Math. Biophys.* 29:657–664.
9. Reitz, J., F. Milford, and R. Christy. 1980. Foundations of Electromagnetic Theory. Addison-Wesley Publishing Co., Reading, MA. 169.
10. Stegeman, D., J. De Weerd, and E. Eijkman. 1979. A volume conductor study of compound action potentials of nerves in situ: the forward problem. *Biol. Cybernetics.* 33:97–111.
11. Roth, B., and J. P. Wikswo. 1985. The electrical potential and magnetic field of an axon in a nerve bundle. *Math. Biosci.* In press.
12. Gelernter, H., and J. Swihart. 1964. A mathematical-physical model of the genesis of the electrocardiogram. *Biophys J.* 4:285–301.
13. Kao, C. Y. 1960. Postsynaptic electrogenesis in septate giant axons. II. Comparison of medial and lateral giant axons of Crayfish. *J. Neurophysiol.* 23:618–635.
14. Leifer, M., and J. P. Wikswo. 1983. Optimization of a clip-on SQUID current probe. *Rev. Sci. Instrum.* 54:1017–1022.